Kapal: Jurnal Ilmu Pengetahuan dan Teknologi Kelautan
(Kapal: Journal of Marine Science and Technology)
journal homepage : http://ejournal.undip.ac.id/index.php/kapal
2301-9069 (e)
1829-8370 (p)

Experimental Investigation on the Characteristics of Pitch Motion for a Novel SPAR-type FOWT in Regular Waves

Fuad Mahfud Assidiq[1)*], Daeng Paroka[1)], Habibi[1)], Hidayatullah[1)], Muhammad Fajar Fitra Ramadan[1)]

[1)] Department of Ocean Engineering, Universitas Hasanuddin, Gowa 92119, Indonesia
[*)] Corresponding Author : assidiqfm@unhas.ac.id

Article Info

Keywords:
Pitch motion;
SPAR;
Vertical Plate;

Article history:
Received: 31/01/2023
Last revised: 08/04/2023
Accepted: 12/05/2023
Available online: 12/05/2023
Published: 17/05/2023

DOI:
https://doi.org/10.14710/kapal.v20i2.52191

Abstract

Pitching mode is more crucial than heaving mode in assessing floating offshore wind turbine (FOWT) motion characteristics, especially the operation of the SPAR substructure. The aim of this paper is to develop an experimental method for improving the SPAR substructure to minimize unnecessary pitch motion. Toward this end, three vertical plate configurations based on the novel SPAR are being developed, known as the 3VP, 4VP, and 5VP models. In consideration of 0º , 30º , 60º , 90º - incidence, the pitch response characteristics of the proposed novel SPAR models are comprehensively evaluated in terms of submerged volume ratio, wave-induced motion, non-dimensional damping coefficient, and percentage of motion reduction. The model test results indicate that the 4VP model outperforms the other novel models with respect to dynamic response, particularly the incidence of 0º and 90º . This study implies that the novel SPAR development is both feasible and effective in the modification of SPAR-type FOWT substructures.

1. Introduction

Renewable energy has expanded in interest in recent times as a primary indicator of ecologic prevention priorities [1]. Wind energy is one of the most extensively utilized renewable energy sources [2], and floating offshore wind turbine (FOWT) facilities are believed to be a leading light in highlighting cost benefits for moderate water depths [3], [4], [5], and the stiffness of the mooring system is relatively lower than a fixed offshore wind turbine [6]. It should be stated that FOWT substructures are classified into three categories: tension leg platform (TLP), semi-submersible, and single point anchor reservoir (SPAR) [7]. In striking contrast to semi-submersible and TLP, the SPAR substructure is frequently selected due to its simple design and excellent stability [8], [9]. Besides this, it features a small water plane area, a deep draft to decrease wave loads, and a natural period added benefit [10].

Despite their accelerated commercial viability, floating platforms possess high fluctuations in highly integrated wave-wind-current loading [11]. Pitching mode is one of the most crucial motions in terms of aerodynamic unsteadiness [12]. Furthermore, the aerodynamic impacts of offshore wind turbine blades are more destructive than those of onshore wind turbine blades, considering dynamic turbulence and lack of alignment [13], [14]. The progress of the floating platform significantly enhances the efficiency of the turbine system overload [15]. The interaction of both the blade and the wake structure is mostly complicated, which can induce vortex rings to represent on a regular basis [16], [17], [18]. The tip speed ratio (TSR), phase difference between the coupled motion (surge and pitch), and the incident wave is heavily affected by pitch motion. It was discovered that low TSR decreases as the reduced frequency increases. Surprisingly, high TSR expanded with lower frequency as well. The power variation spreads in immediate proportion to the boost in TSR [19]. This indicates that anomalies in power performance exist. Furthermore, the phase difference event demonstrates that increasing pitch motion can diminish the power generated. Turbine blades in the coupled motion phase are classified as severe: vortex ring state or propeller state [20]. This phase difference would further adjust the behavior of the substructure as the power generated fluctuates.

Several modifications to existing substructures such as stepped-SPAR, counterweight disc, and heave plate are offered as alternatives. Initially, the stepped-SPAR model demonstrated numerous strengths over the base SPAR, including acceptable hydrodynamic performance based on turbulent winds, the use of a 4 x 1 mooring pattern as active pitch damping, and the possibility to be implemented in moderate waters for potential savings [6], [21], [22]. Likewise, compared without disc usages, counterweight disc technology could really derive additional added mass, damping, and

decreasing of heave motion [23]. Heave plates, the same as the previous technology, are a quick fix for increasing vertical damping and yet are perfectly suited to FPSOs or mono column structures [9], [24], [25], [26], [27]. All of them are hardly possible to reduce the massive heave motion insufficiently.

To the finest of the authors' expertise, vertical plates are the most advanced SPAR damping solution. This is attributable to the fact that pitch motion damping is more important than heave motion damping [28]. It is feasible to realize sufficient pitch motion reduction through using four vertical plates instead of heave plates, as strongly advised in their investigation. However, once four vertical plates are not equalized with the number of other vertical plates, they serve ambiguous. The evidence provided in this study is devoted to investigating the pitch motion characteristics of a novel SPAR in regular waves using several vertical plate configurations. The paper proceeds by outlining the experiments of the novel SPAR model and simulation circumstances in Section 2. Section 3 represents a detailed analysis and discussion of the pitch response, frequency ratio, non-dimensional damping, and pitch reduction percentage. Finally, Section 4 concludes it.

2. Methods

Model testing took place at Ocean Technology Laboratory in Universitas Hasanuddin, Indonesia. The 24 x 1.0 x 1.1 m wave tank was fully equipped with a wave maker within one side and a wave absorber at the opposite to construct and eliminate the implemented waves, as demonstrated in Figure 1. Especially considering the SPAR model sizes and wave tank features, as depicted in Figure 2, the scale carefully selected for SPAR prototype is 1:115, which accurately predicts structural dynamics and hydrodynamics. As a benchmark in this investigation, a detailed dataset on the dimensionality of the 6 MW base SPAR is reviewed in [29], [30]. Because 17.7 x 5.0 x 1.5 m vertical plates of the novel SPAR are the main parameters in this study, configurations of three vertical plates (3VP), four vertical plates (4VP), and five vertical plates (5VP) are compared to the base SPAR model, as shown in Figure 3. Table 1 displays the scaling laws and wave parameters of the SPAR model. Further observed wave parameters are identified in [31]. Therefore, indeed the pitch criterion is utilized to identify the degree of tilt as illustrated in Figure 4. To precisely satisfy the scalability relationship, the SPAR system was designed of polyvinyl chloride (PVC), cement to handle the fixed ballast volume, and a tether made of a flexible rubber string to restrict the model from drifting. Moreover, the model was centered within the wave tank sizes in a 0.7 m-scaled water depth. The pitch motion of the model was also closely monitored using a gyroscope tracking solution. The test conditions involve a pitch decay test and a regular wave test. The decay test was executed in still water without a wave excitation disturbance. The aim of this test is to examine the natural period and non-dimensional damping of various SPAR models. The regular wave test greatly helps in gaining an initial comprehension of the behavior of all novel SPAR models under different wave parameters for 120 seconds. Wave incidence was evaluated at 0º , 30º , 60º , and 90º to assess the difference in pitch response. The Cartesian coordinate system at the center of mass was adopted to decide the wave incidence, as displayed in Figure 5.

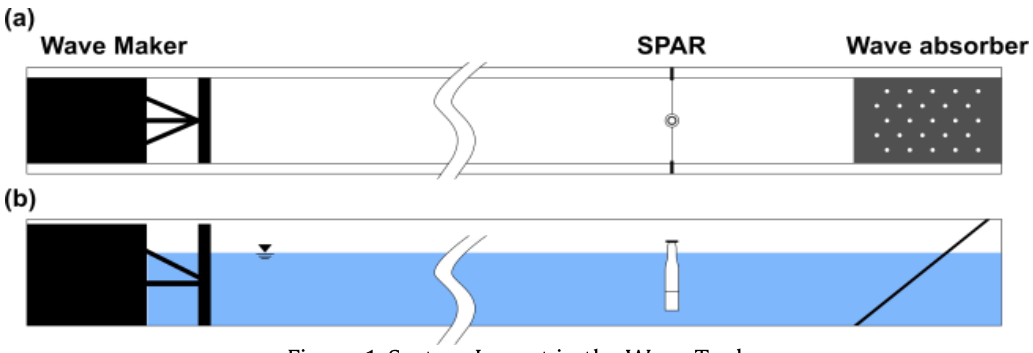

Figure 1. System Layout in the Wave Tank

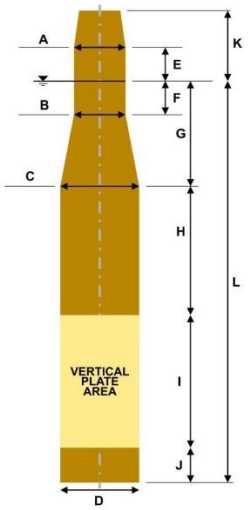

Codes	Values
A	8.0
B	9.5
C	14.6
D	6.0
E	6.0
F	20.0
G	29.1
H	4.6
I	17.7
J	4.6
K	13.0
L	76.0

*units: m

Figure 2. Particulars of the Novel SPAR

Figure 3. 6 MW Base SPAR versus Novel SPAR Concepts

Table 1. Regular Wave Testing Conditions

Load Cases	Real Scale		Model Scale		Incidences
	H (m)	T (s)	H (m)	T (s)	
LC #1	2.0	10.724	0.017	1.0	0º , 30º , 60º , & 90º
LC #2	4.0	12.869	0.035	1.2	
LC #3	6.0	15.013	0.052	1.4	

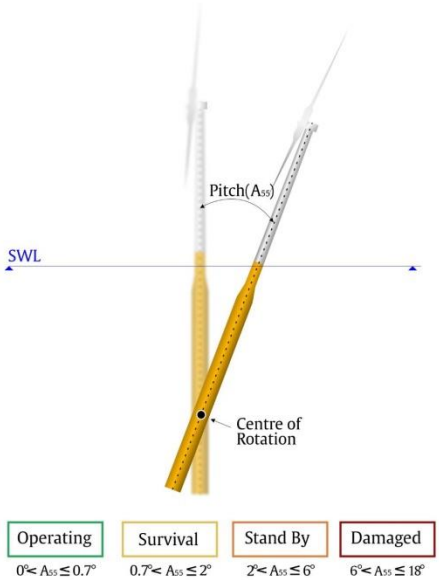

Figure 4. Sketch of Pitch Response when SPAR Tilts

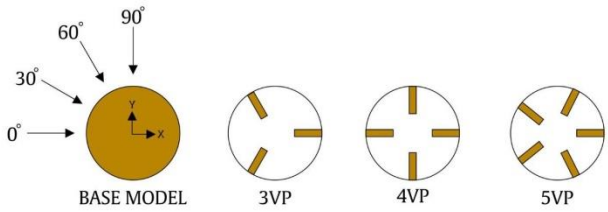

Figure 5. Top View Cross-section of the Models and the Incidence Angle of Waves

3. Results and Discussion

3.1. Submerged Volume Ratio (V_r)

Figure 6 depicts the effect of submerged volume ratio (V_r) on pitch response at 0º , 30º , 60º , and 90º incidence. The pitch motion was classified using statistical analysis based on the maximum, minimum, mean, and standard deviation. The submerged volume ratio is calculated by comparing the submerged volume in the ballast area between the base model and the novel SPAR with vertical plate replacement. It should be noted that the 3VP model has the lowest V_r ratio, while the base model has the highest. In Figure 6(a-b-c), the pitch response statistically follows a similar pattern with increasing wave parameters, in this case for all load cases. This pattern demonstrates that the 0º incidence allows for quick recognition of the pitch response. Furthermore, the best pitch motion is revealed by submerged volume ratios of 0.18, 0.22, 0.13, and 1.00. At this point, the pitch responses of all SPAR models meet the stand-by and damaged criteria.

Figure 6 (d-e-f) depicts the statistical pitch response of all submerged volume ratios at 30º -incidence. The pitch response trend differs significantly in each increasing load case. The difference occurs at various submerged volume ratios. This is because the 30º incidence has a large influence on the pitch response, so it is critical to carefully observe the applied load case based on the future installation location. Submerged volume ratios of 1.00, 0.13, 0.18, and 0.22, for example, are capable of reducing pitch motion well in load case 1 (LC #1). In comparison to the other models, the model with V_r = 1.00 has a very large reduction difference. This means it works extremely well. All SPAR models meet the stand-by and damaged criteria in this load case. On the other hand, different models were discovered that produced the smallest pitch response during LC #2. The ratio is in the following order: 1.00, 0.22, 0.13, and 0.18. The damaged criterion applies to all models. Similarly to LC #1, the model with V_r = 1.00 shows a significant difference in minimizing pitch response when compared to the other models. In LC #3, the pitch response is minimized at ratios of 0.18, 1.00, 0.22, and 0.13, respectively. All SPAR models are classified as damaged as a result of this load case.

Except for load case 1 (LC #1) in Figure 6(g-h-i), the pitch response statistically follows a similar pattern with increasing load case within 60º incidence. This is because, when large wave parameters are taken into account, incidence has a significant impact on pitch response generation. Looking closely at LC #1, the model value between Vr = 0.13 and 1.00 is only a hair away apart. This means that the largest and smallest submerged volume ratios can reduce excessive pitch motion together. As a result, when the ratios are sorted, the smallest pitch is seen at 1.00, 0.13, 0.18, and 0.22, respectively.

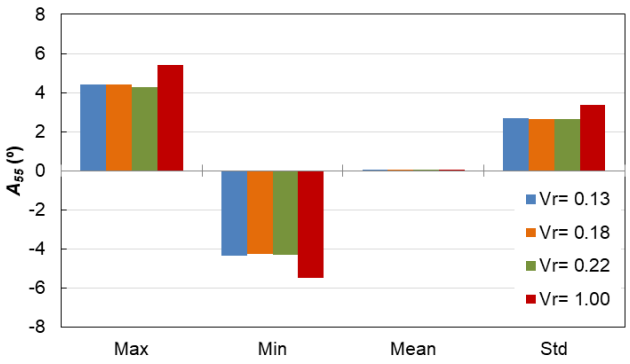

(a) 0º - LC #1

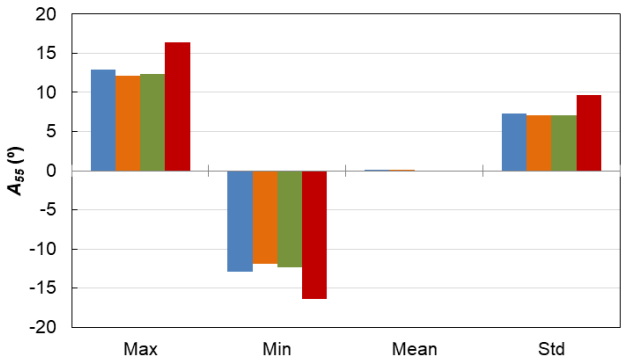

(b) 0º - LC #2

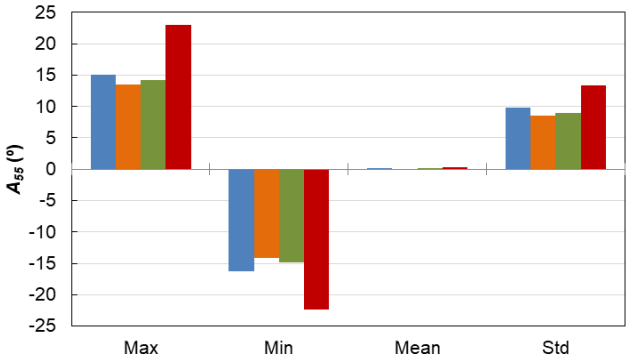

(c) 0º - LC #3

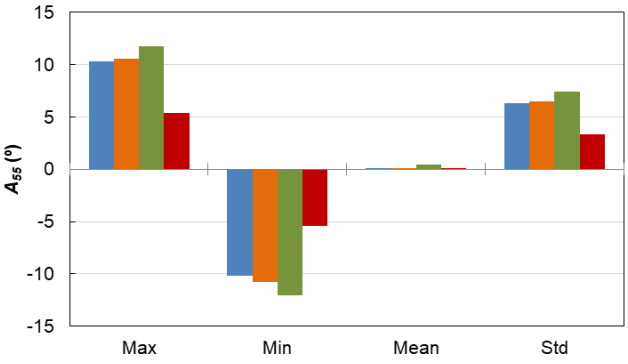

(d) 30º - LC #1

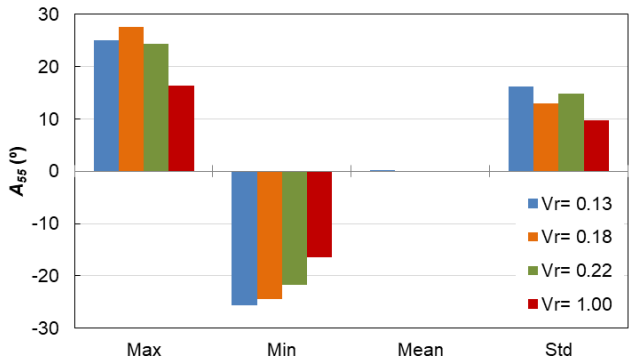

(e) 30° - LC #2

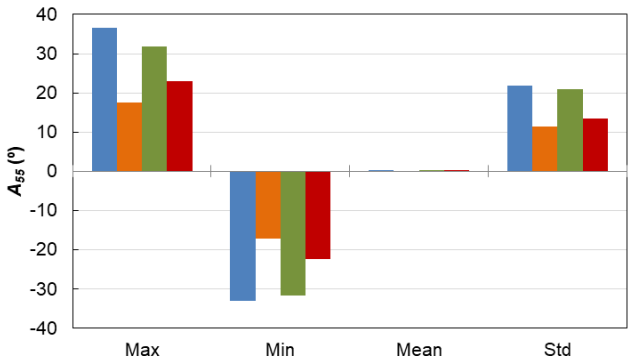

(f) 30° - LC #3

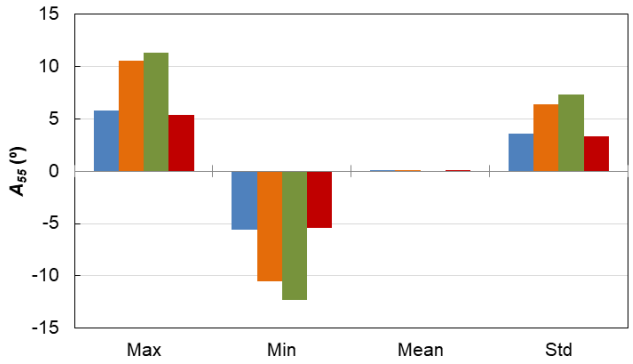

(g) 60° - LC #1

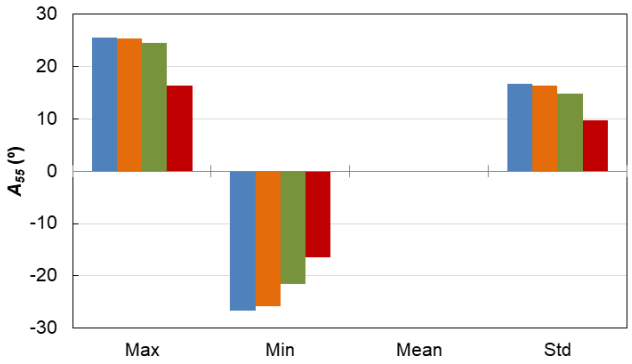

(h) 60° - LC #2

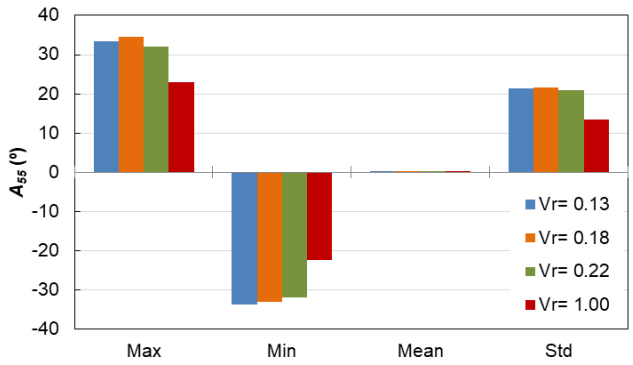

(i) 60° - LC #3

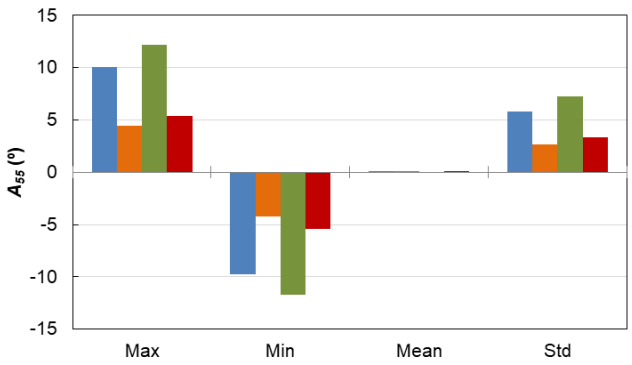

(j) 90° - LC #1

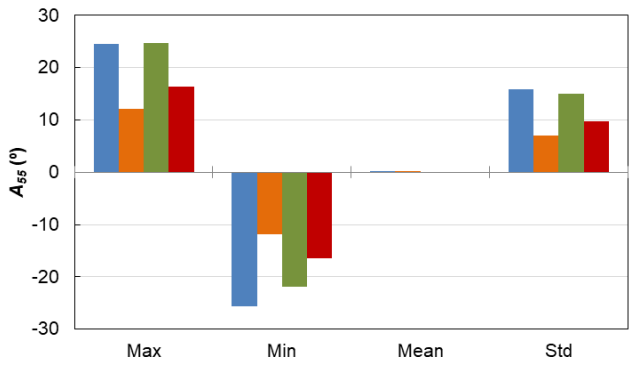

(k) 90° - LC #2

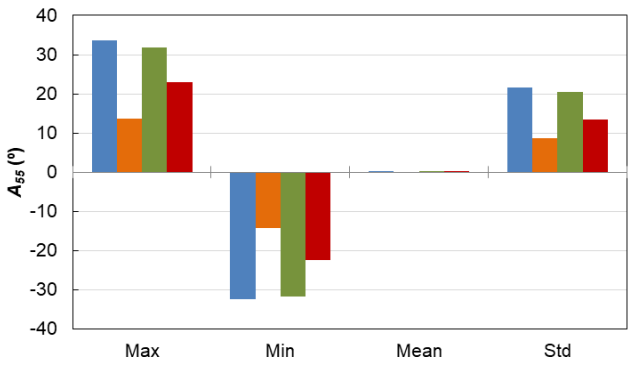

(l) 90° - LC #3

Figure 6. Statistical Pitch Responses of Submerged Volume Ratios at Different Both Load Cases and Incidences

The pitch response of all SPAR models falls into the stand-by and damaged criteria in this load case. Unlike LC #2, it appears very different from LC #1, with the exception of V_r = 1.00, where the pitch response is very small compared to others. As a result, the submerged volume ratios of 1.00, 0.22, 0.18, and 0.13 are the most effective at reducing pitch motion. All SPAR models are classified as damaged as a result of the application of this load case. Similar to LC #2, the difference in submerged volume ratio of LC #3 only contrasts during the highest pitch response. This means that the large

wave parameter of 60º -incidence makes pitch motion estimation effortless. The smallest pitch sequences are seen at ratios of 1.00, 0.22, 0.13, and 0.18, respectively. Furthermore, all models are affected by the damaged criterion.

In Figure 6(j-k-l), the pitch response follows a similar pattern with increasing load cases at 90º -incidence. The LC #3 condition, on the other hand, displays a slightly different pattern. All of these trends indicate that the pitch response is rather easy to recognize at 90 degrees incidence. Moreover, submerged volume ratios of 0.22, 0.22, 0.13, and 1.00 provide the best pitch motion under LC #1 and LC #2 conditions, respectively. The smallest pitch sequence of LC #3, on the other hand, was identified at ratios of 0.13, 0.22, 1.00, and 0.18, respectively. In all cases, the pitch responses of all SPAR models fulfill the stand-by and damaged criteria. As a matter of fact, it is strongly advised that the pitch motion be mitigated by finding the SPAR model's submerged volume ratio into account. Even so, appropriate assessment of the incidence is expected for the SPAR to operate properly.

3.2. Wave-induced Pitch Motion

The natural period (T_n) of the SPAR must first be ascertained through free-decay testing before the oscillation behavior can be identified. The pitch free-decay test begins with an initial inclination of 15º . Figure 7 depicts all novel SPAR wind floaters that were tested at various angles of incidence and produced high natural period in comparison to the base model. This is because the base model had a low viscous damping per oscillation cycle during the free-decay test. Under 0º of incident angle, the addition of vertical plates to the novel SPAR results in a concomitant increase in natural period. Notably, the difference in natural period between the 4VP and 5VP models is not significant. The highest natural period is achieved in this instance by the 5VP model. At 30º and 60º incidence, however, all novel SPARs produced insignificant natural period differences. Model 3VP is slightly better than the others. At 90º incidences, the 4VP model far outperforms the others. This all suggests that the influence of the number of vertical plates in natural period consideration is barely perceptible.

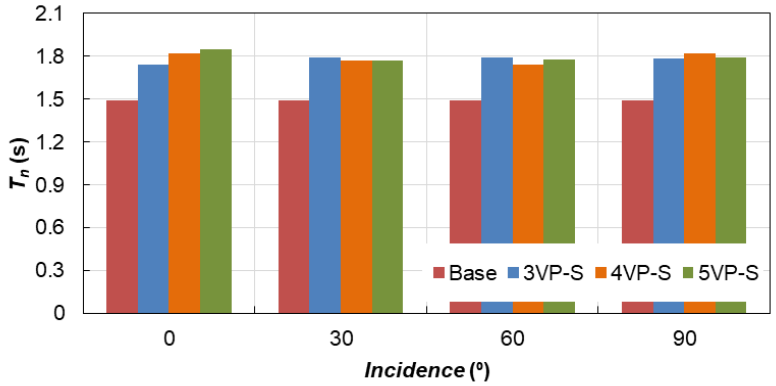

Figure 7. Pitch Natural Periods from Free-decay Test at Different SPAR Models

To simplify the discrepancy of SPAR motion distribution, the application of pitch nominal amplitude ($A_{n\,55}$) to reduced velocity ($U_r = \frac{(U.T_n)}{D}$, where $U = \frac{\pi.H}{T}$) is detailed in Figure 8 for all novel SPAR models compared to the base model [32], [33], [34] and in Figure 9 for angle of incident range classification. With reference to Figure 4, all models are in standby and damaged condition. It is also demonstrated that all SPAR models form an increasing curve as U_r increases. Furthermore, the findings show that the position of the vertical plate configuration has a significant impact on the angle of incidence. Figure 8(a) shows that the 3VP model produces the lowest amplitude when compared to the base model only at 0 degrees. Meanwhile, the enhancement of the $A_{n\,55}$ curve follows a slightly different pattern in the 30º , 60º , and 90º incidences. The distinction appears only when U_r is greater than 0.70. Figure 8(b) shows that the 0º and 90º incidences alone produce the smallest $A_{n\,55}$ when compared to the base model. Another thing to keep in mind is that the curve decreases at 30º because U_r is greater than 1.10. Furthermore, the greatest $A_{n\,55}$ curve occurs only at 60º . Figure 8(c) shows that the 0º incidence produces the smallest $A_{n\,55}$ when compared to the base model. The incidences of 30º , 60º , and 90º , on the other hand, exhibit a slightly different trend in the increase of the $A_{n\,55}$ curve. When U_r is greater than 1.60, the difference appears.

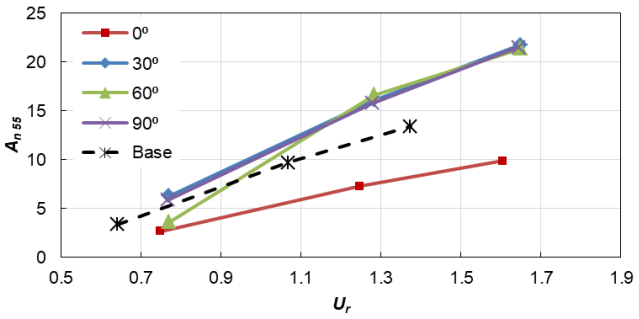

(a) 3VP Model

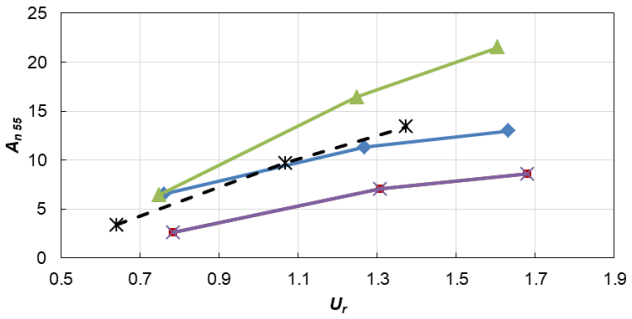

(b) 4VP Model

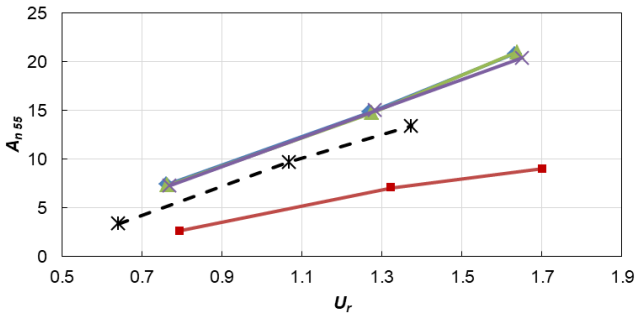

(c) 5VP Model

Figure 8. Characteristic Amplitudes of the Pitch Responses for All Incidences at Different Novel SPAR Models

Figure 9(a-b-c-d) compares all SPAR models in terms of incident angle, as discussed previously. Figure 9(a) shows that the 4VP and 5VP models have the smallest $A_{n\,55}$ values at 0° . The difference, however, occurs when U_r is greater than 1.70. The $A_{n\,55}$ of the 3VP model is then in third place. An intriguing point can be found in the base model where the difference with the novel SPAR model is significant. This shows that the vertical plate works effectively at this incident angle. Figure 9(b) depicts the $A_{n\,55}$ in the 30° incidence. Starting around $U_r \approx$ 1.10, the 4VP model becomes the smallest $A_{n\,55}$ value model. Despite the fact that the base model's smallest $A_{n\,55}$ appears before $U_r \approx$ 1.10 as well. The difference in $A_{n\,55}$ between the 3VP and 5VP models, on the other hand, is less pronounced than that of the other models. This results in the vertical plate having little effect at the 30° condition in this case only for the 4VP model. Figure 9(c) depicts the $A_{n\,55}$ with respect to the 60° condition. It's worth noting that the smallest $A_{n\,55}$ is found only in the Base model. The difference in motion between the novel SPAR models and the base model is noticeably less pronounced in all of them. The 60° incidence factor has the greatest influence on the less effective reduction of $A_{n\,55}$. Figure 9(d) depicts the $A_{n\,55}$ in a 90° incidence. In comparison to other SPAR models, model 4VP has the lowest $A_{n\,55}$ value. Its $A_{n\,55}$ value remains far from the closest SPAR model curve. The difference in $A_{n\,55}$ between the 3VP and 5VP models, on the other hand, is barely discernible. Similarly, the base model is nearly identical to the two SPAR models. Because of this, the vertical plate only affects the 4VP model at 90° . Finally, based on the standard deviation of pitch motion, it is discovered that the effect of incident angle is largely determined by the vertical plate configuration.

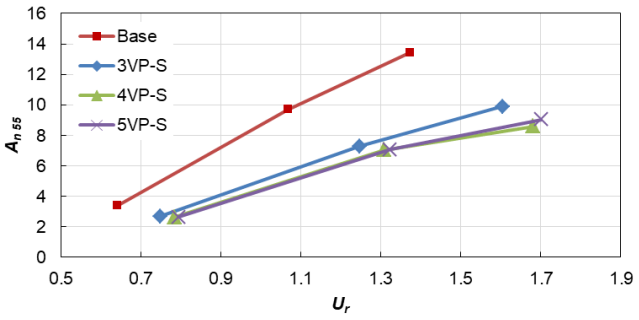

(a) 0° - Incidence

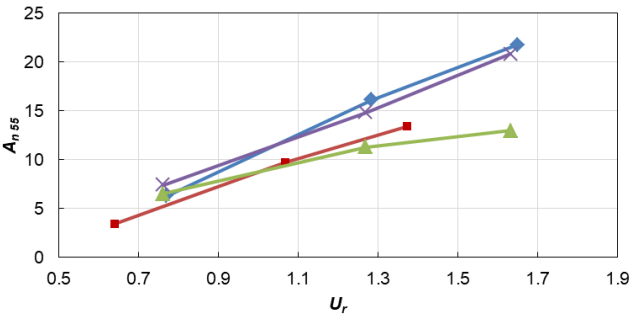

(b) 30° - Incidence

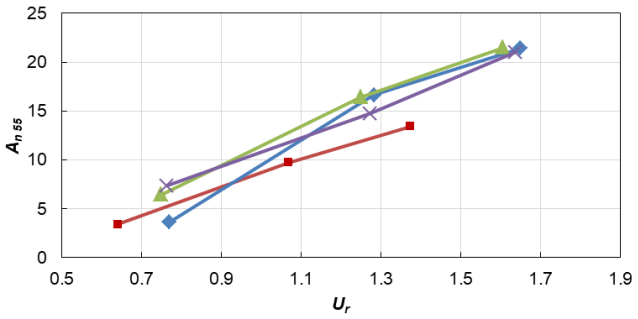

(c) 60° - Incidence

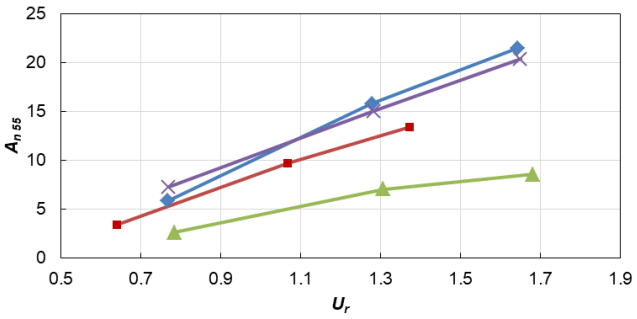

(d) 90° - Incidence

Figure 9. Comparison of SPAR Models in Characteristic Amplitudes of the Pitch Responses at Different Incidences

The implementation of the frequency ratio ($\frac{f_p}{f_n}$, where f_p is the pitch mode vibration frequency and $f_n = \frac{1}{T_n}$ denotes natural frequency) to the reduced velocity U_r is shown in detail in Figure 10 to prevent pitch resonance mode due to wave-induced pitch motion [32]. All models are above the dashed line of the resonant behavior, refered to as lock-in$\left(\frac{f_p}{f_n} = 1.00\right)$. It is also demonstrated that as U_r increases, all SPAR models form a gradually decreasing curve. Only the base model is closest to the resonance zone at all angles of incident testing. This implies that the pitch motion of the base model should be significant. Furthermore, vortex shedding is observed to be more likely as the wave parameter increases with respect to various angles of incidence.

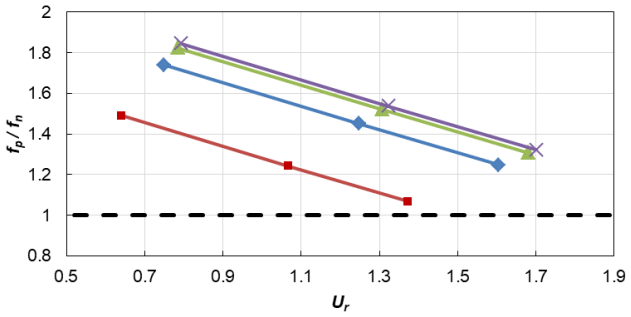

(a) 0° - Incidence

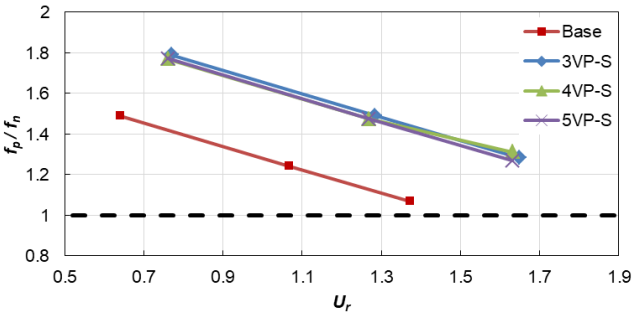

(b) 30° - Incidence

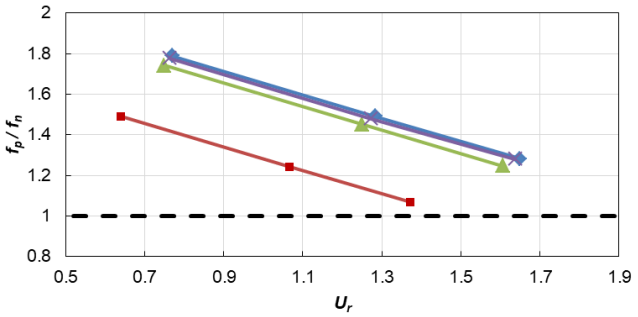

(c) 60° - Incidence

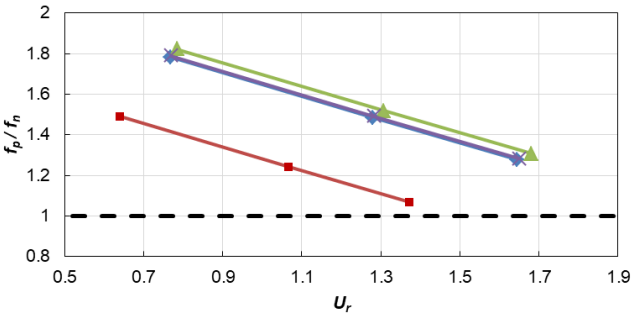

(d) 90° - Incidence

Figure 10. Frequency Ratio for SPAR Models at Different Incidences, the Dashed Line Represents the Lock-in Phenomenon

Figure 10(a) depicts the frequency ratio frequency ratio with respect to the 0° incidence. In comparison to other SPAR models, the 5VP model has the highest frequency ratio value. The following orders are 4VP and 3VP, respectively. Also, the greater the number of vertical plates, the higher the frequency ratio. Figure 10(b) depicts frequency ratio in the 30° incidence. All of the novel SPAR models are mutually exclusive. This confirms that frequency ratios are nearly identical in terms of preventing vortex shedding. Figure 10(c) depicts frequency ratio toward 60° , where model 3VP is slightly superior to model 5VP. In comparison to 30° , the 4VP model is more similar to the two previous models. As a result, when compared to the 3VP and 5VP models, the 4VP model is quite weak at preventing vortex shedding. In fact, in contrast to the 60° case, the 4VP model outperforms the 3VP and 5VP models in terms of frequency ratio, as shown in Figure 10(d). Even the difference in the 60° incidence tends to be similar. Furthermore, the 5VP model outperforms the 3VP model marginally. This is why the angle of incidence produces such a noticeable difference in the frequency ratio of each SPAR model. As a result, this subsection demonstrates that the vertical plate effectively reduces the vortex phenomenon.

3.3. Pitch Damping Coefficient Effect (K)

Figure 11 depicts the implementation of the non-dimensional damping coefficient (K) considering the keel to center of buoyancy (K_B) to recognize the crucial role of submerged volume configurations in pitch damping motion. This damping is calculated from the measurement of several guideline amplitudes during the pitch free-decay test; see the related study for more information [35], [36]. These vertical distance terminologies of 0.171, 0.227, 0.229, and 0.232 are representative of the Base, 5VP, 4VP, and 3VP models, respectively. It is discovered that non-dimensional damping coefficient is not always proportional to the K_B. Furthermore, regardless of the angle of incidence, all novel SPAR models produce significant non-dimensional damping coefficient when compared to the base model. The best damping was revealed by the 5VP, 4VP, and 3VP models, respectively.

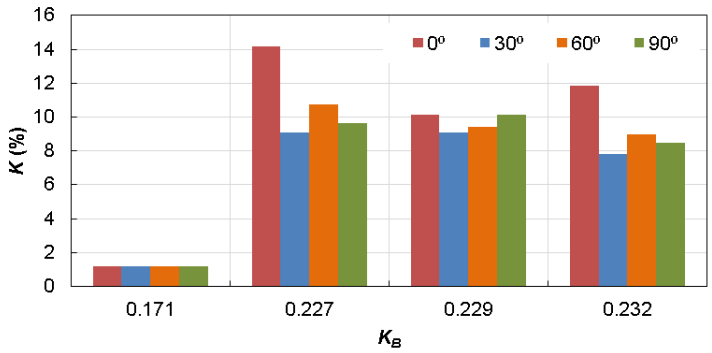

Figure 11. Non-dimensional Damping Coefficient for Keel to Center of Buoyancy at Different Incidences

3.4. Pitch Response Reduction (P_r)

Figure 12 depicts the effect of wave slope $\left(\frac{H}{gT^2}\right)$ on the pitch reduction percentage comparison between the novel SPAR and base model (P_r). The maximum pitch value of each SPAR model is represented by the pitch reduction motion. This is greatly influenced not only by the wave height and period, but also by the angle of incidence. It can even help reduce the SPAR submerged volume, as discussed in the previous subsection. Figure 12(a) depicts the pitch mode reduction with the wave slope set to 0° . At this incident angle, as the wave inclination increases, so does the percentage reduction. The best novel SPAR models capable of producing the greatest percentage reduction are the 4VP, 5VP, and 3VP models, respectively. Since the wave slope is small, the 5VP model outperforms the 3VP and 4VP models slightly. However, at large wave slopes, the percentage reduction of the 4VP model is greater than the 3VP and 5VP models. The pitch mode reduction in the incidence of 30° with respect to the wave slope is depicted in Figure 12(b). At this incident angle, as the wave slope increases, so does the percentage reduction. When ranked, the 4VP, 5VP, and 3VP models produce the greatest percentage reduction. It is also worth noting that the highest reduction percentages for each increase in wave slope differ between SPAR models. However, in this case, it can be seen that the dominant novel SPAR model is unable to significantly reduce pitch motion. The reduction of pitch motion is, as is well known, negative. In fact, the 4VP model can only reduce motion when the wave slope is extremely steep. Figure 12(c) depicts the pitch mode reduction with the wave slope at 60° in mind. 5VP, 3VP, and 4VP are the best novel SPAR models capable of producing the highest percentage reduction. It was discovered that increasing wave slope does not always increase the percentage of reduction at this incident angle. This occurred in the 3VP model, where the pitch reduction curve decreased dramatically. In fact, all reduction percentages are negative. This implies that none of the novel SPAR models can significantly reduce pitch motion in this incidence. Figure 12(d) depicts the pitch mode reduction at 90° to the wave slope. Similarly to the 0° and 30° incidence, the percentage reduction increases as the wave slope increases. The best novel SPAR models capable of producing the greatest percentage reduction when ranked are the 4VP, 3VP, and 5VP models, respectively. Unless the wave slope is lesser, the 4VP model outperforms the 3VP and 5VP models. At large wave slopes, nevertheless, the percentage reduction of the 4VP model is greater than the other models. Only the 4VP model can suppres pitch motion, which is an intriguing point. Regardless of the fact that the other models contribute even less to the prevention of excessive pitch motion. Ultimately, compared to other incidences, only the 0° incidence could really provide an efficient reduction effect on the entire novel SPAR. With respect to the angle of incidence, the vertical plate configuration has a greater influence.

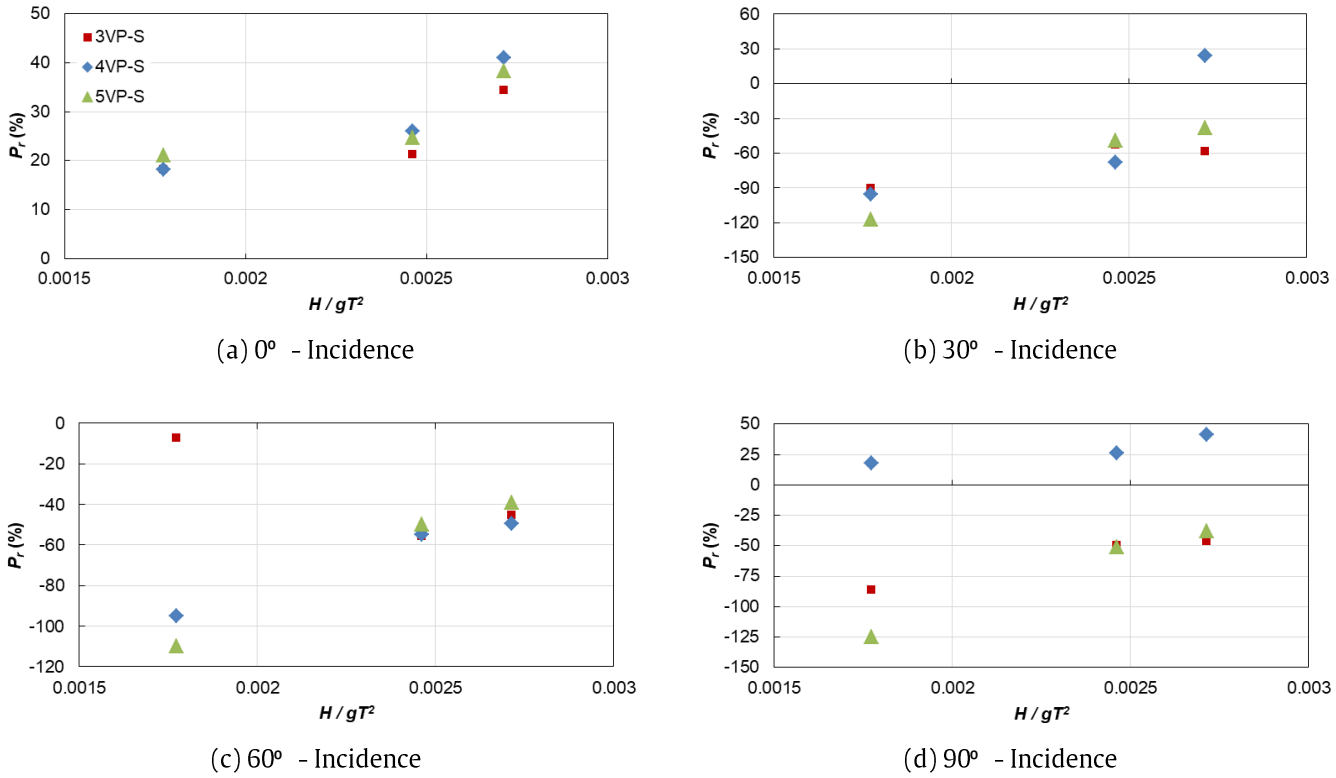

(a) 0° - Incidence (b) 30° - Incidence

(c) 60° - Incidence (d) 90° - Incidence

Figure 12. Pitch Response Reductions of Three Novel SPARs considering Base Model at Different Incidences

4. Conclusion

The effect of the vertical plate configuration is examined experimentally in this paper. The submerged volume ratio V_r, wave-induced pitch motion, non-dimensional pitch damping coefficient K, and pitch motion reduction P_r are all investigated. The following conclusions were drawn:

1. In comparison to wave parameters, the submerged volume ratio is the most influential concern for proportionally assessing pitch response performance. Nevertheless, it has obstacles in rapidly figuring out the ratio to demonstrate the accuracy of the SPAR model through considering of all incidences. As a logical consequence, the generated submerged volume ratio is acceptable for use during moderate waters, especially in estimating engineering cost savings.
2. The wave-induced pitch motion has been closely related to the natural period, nominal pitch amplitude, and frequency ratio. The difference in the natural period T_n of all the novel SPAR models generated is infinitesimal, and yet it exceeds the base model by a large margin. Moreover, the angle of incidence will undoubtedly affect the pitch nominal amplitude $A_{n\ 55}$ for all three novel SPAR models. On this justification, it also constitutes iconic proof that the vertical plates of novel SPAR models can effectively mitigate the vortex shedding phenomenon.
3. The keel to center of buoyancy has a great impact on the non-dimensional damping coefficient of the pitch subjected to all incidences. The damping coefficient increases dramatically as the keel to buoyancy decreases, except K_B= 0.171 which indicates the base SPAR. The greatest non-dimensional damping coefficient is observed at 0° incidences, while the smallest clearly shows at 30° incidences.
4. The performance of pitch reduction percentage with respect to the base SPAR varies depending on the incident direction of the wave slope. The 4VP model conducts well in percentage terms, particularly for 0° incidences. Models 3VP and 5VP tend to have percentage reduction limitations, even generating potential losses at incidences of 30° , 60° , and 90° .

It should be confirmed that only some wave parameters were nominated for this study, and their applicability is highly dependent on the desired sea state. Consequently, since the tests are still being conducted on a regular response based, the findings may be slightly conservative. The selected SPAR, the 4VP model, is derived from the four issues outlined in the previous section. Future research needs to concentrate on improving a more tangible vertical plate depending on the aspect ratio and platform construction planning. It will be approximated in investigating the pitch motion characteristics in depth.

Acknowledgements

This work was funded by the Novice Lecturer Research Program (PDPU) – LPPM Universitas Hasanuddin (Grant No. 1477/UN4.22/PT.01.03/2022). In the end, the authors are grateful to reviewers for their thorough understandings and insightful suggestions, which substantially improved the work's quality.

References

[1] L. Meng, T. Zhou, Y. He, Y. Zhao, and Y. Liu, " Concept design and coupled dynamic response analysis on 6-MW spar-type floating offshore wind turbine," *China Ocean Engineering*, vol. 31, no. 5, pp. 567– 577, 2017.

[2] B. K. Sahu, " Wind energy developments and policies in China: A short review," *Renewable and Sustainable Energy Reviews*, vol. 81, pp. 1393– 1405, 2018.

[3] S. Bashetty and S. Ozcelik, " Review on Dynamics of Offshore Floating Wind Turbine Platforms," *Energies*, vol. 14, no. 19, p. 6026, 2021.

[4] X. Wu., Y. Hu., Y. Li., J. Yang., L. Duan., T. Wang., T. Adcock., Z. Jiang., Z. Gao., Z. Lin., A. Borthwick., S. Liao " Foundations of offshore wind turbines: A review," *Renewable and Sustainable Energy Reviews*, vol. 104, pp. 379– 393, 2019.

[5] G. Stewart and M. Muskulus, " A Review and Comparison of Floating Offshore Wind Turbine Model Experiments," *Energy Procedia*, vol. 94, pp. 227– 231, 2016.

[6] T. Wen, K. Wang, Z. Cheng, and M. Ong, " Spar-Type Vertical-Axis Wind Turbines in Moderate Water Depth: A Feasibility Study," *Energies*, vol. 11, no. 3, p. 555, 2018.

[7] M. Karimirad and T. Moan, " A simplified method for coupled analysis of floating offshore wind turbines," *Marine Structures*, vol. 27, no. 1, pp. 45– 63, 2012.

[8] H. M. Johlas, L. A. Martínez- Tossas, M. J. Churchfield, M. A. Lackner, and D. P. Schmidt, " Floating platform effects on power generation in spar and semisubmersible wind turbines," *Wind Energy*, vol. 24, no. 8, pp. 901– 916, 2021.

[9] T. D. Pham and H. Shin, " A New Conceptual Design and Dynamic Analysis of a Spar-Type Offshore Wind Turbine Combined with a Moonpool," *Energies*, vol. 12, no. 19, p. 3737, 2019.

[10] J. Chen and M.-H. Kim, " Review of Recent Offshore Wind Turbine Research and Optimization Methodologies in Their Design," *Journal of Marine Science and Engineering*, vol. 10, no. 1, p. 28, 2021.

[11] Z. Jiang., B. Wen., G. Chen., L. Xiao., J. Li., Z. Peng., X. Tian, " Feasibility studies of a novel spar-type floating wind turbine for moderate water depths: Hydrodynamic perspective with model test," *Ocean Engineering*, vol. 233, p. 109070, 2021.

[12] T. Sebastian, " The Aerodynamics and Near Wake of an Offshore Floating Horizontal Axis Wind Turbine," Ph.D Thesis, University of Massachusetts Amherst, Amherst, 2012.

[13] T. Sebastian and M. Lackner, " Analysis of the Induction and Wake Evolution of an Offshore Floating Wind Turbine," *Energies*, vol. 5, no. 4, pp. 968– 1000, 2012.

[14] T. Sebastian and M. A. Lackner, " Characterization of the unsteady aerodynamics of offshore floating wind turbines," *Wind Energy*, vol. 16, no. 3, pp. 339– 352, 2013.

[15] M. Jeon, S. Lee, and S. Lee, " Unsteady aerodynamics of offshore floating wind turbines in platform pitching motion using vortex lattice method," *Renewable Energy*, vol. 65, pp. 207– 212, 2014.

[16] S. Rockel, E. Camp, J. Schmidt, J. Peinke, R. Cal, and M. Hölling, " Experimental Study on Influence of Pitch Motion on the Wake of a Floating Wind Turbine Model," *Energies*, vol. 7, no. 4, pp. 1954– 1985, 2014.

[17] S. Rockel, J. Peinke, M. Hölling, and R. B. Cal, " Wake to wake interaction of floating wind turbine models in free pitch motion: An eddy viscosity and mixing length approach," *Renewable Energy*, vol. 85, pp. 666– 676, 2016.

[18] P. Cheng, Y. Huang, and D. Wan, " A numerical model for fully coupled aero-hydrodynamic analysis of floating offshore wind turbine," *Ocean Engineering*, vol. 173, pp. 183– 196, 2019.

[19] B. Wen, X. Dong, X. Tian, Z. Peng, W. Zhang, and K. Wei, " The power performance of an offshore floating wind turbine in platform pitching motion," *Energy*, vol. 154, pp. 508– 521, 2018.

[20] X. Feng, Y. Lin, G. Zhang, D. Li, H. Liu, and B. Wang, " Influence of Combined Motion of Pitch and Surge with Phase Difference on Aerodynamic Performance of Floating Offshore Wind Turbine," *Journal of Marine Science and Engineering*, vol. 9, no. 7, p. 699, 2021.

[21] T. Utsunomiya., H. Matsukuma., S. Minoura., K. Ko., H. Hamamura., O. Kobayasahi., I. Sato., Y. Nomoto., K. Yasui, " On Sea Experiment of a Hybrid SPAR for Floating Offshore Wind Turbine Using 1/10 Scale Model," in *29th International Conference on Ocean, Offshore and Arctic Engineering:* vol. *3*, pp. 529– 536, 2010.

[22] L. Sethuraman and V. Venugopal, " Hydrodynamic response of a stepped-spar floating wind turbine: Numerical modelling and tank testing," *Renewable Energy*, vol. 52, pp. 160– 174, 2013.

[23] T. Seebai, R. Sundaravadivelu, and C. P. Vendhan, " Model Studies on Spar Platform With 5MW Wind Turbine," in *Volume 1: Offshore Technology*, pp. 241– 245, 2009.

[24] I. Amin, S. Dai, S. Day, S. Oterkus, and E. Oterkus, " Experimental investigation on the influence of interceptor plate on the motion performance of a cylindrical FPSO," *Ocean Engineering*, vol. 243, p. 110339, 2022.

[25] P. C. Mello., E.B Malta., R.O.P. da Silva., M.H.O. Candido., L.H.S. do Carmo., I.F. Alberto., G.R. Franzini., A.N. Simos., H. Suzuki., R.T. Goncalves, " Influence of heave plates on the dynamics of a floating offshore wind turbine in waves," *Journal of Marine Science and Technology*, vol. 26, no. 1, pp. 190– 200, 2021.

[26] A. Abazari, M. Alvandi, M. Behzad, and K. P. Thiagarajan, " Vortex shedding modes around oscillating non-uniform double heave plates," *Proceedings of the Institution of Mechanical Engineers, Part M: Journal of Engineering for the Maritime Environment*, vol. 235, no. 2, pp. 558– 569, 2021.

[27] S. Nallayarasu and K. Bairathi, " Hydrodynamic response of spar hulls with heave damping plate using simplified approach," *Ships and Offshore Structures*, vol. 9, no. 4, pp. 418– 432, 2014.

[28] S. Ishida and Y. Imai, " New Spar Design for Floating Offshore Wind Turbine With Damping Plates," in *Volume 9: Rodney Eatock Taylor Honoring Symposium on Marine and Offshore Hydrodynamics; Takeshi Kinoshita Honoring Symposium on Offshore Technology*, 2019.

[29] Y. Jie, H. Y. Ping, Sheng. Zhao Yang, S. Y. Lin, and H. Chong, " Current effect on the hydrodynamic responses of spar type floating offshore wind turbine," *Proceedings of the Thirtieth (2020) International Ocean and Polar Engineering Conference*, pp. 398– 405, 2020.

[30] Z. Zheng, J. Chen, H. Liang, Y. Zhao, and Y. Shao, " Hydrodynamic Responses of a 6 MW Spar-Type Floating Offshore Wind Turbine in Regular Waves and Uniform Current," *Fluids*, vol. 5, no. 4, p. 187, 2020.
[31] M. C. Ong, " CFD applications in offshore engineering," *EPJ Web of Conferences*, vol. 143, p. 01002.
[32] J. Wang, D. Fan, and K. Lin, " A review on flow-induced vibration of offshore circular cylinders," *Journal of Hydrodynamics*, vol. 32, no. 3, pp. 415– 440, 2020.
[33] M. Liu, L. Xiao, Y. Kou, C. Tian, and H. Wei, " Effects of column shape and configuration on the vortex-induced motions of semi-submersibles," *Marine Structures*, vol. 72, p. 102773, 2020.
[34] J. Zhao, J. Leontini, D. lo Jacono, and J. Sheridan, " The effect of mass ratio on the structural response of a freely vibrating square cylinder oriented at different angles of attack," *Journal of Fluids and Structures*, vol. 86, pp. 200–212, 2019.
[35] S.-M. Jeong, B.-H. Son, and C.-Y. Lee, " Estimation of the Motion Performance of a Light Buoy Adopting Ecofriendly and Lightweight Materials in Waves," *Journal of Marine Science and Engineering*, vol. 8, no. 2, p. 139, 2020.
[36] J. M. J. Journée and W. W. Massie, *Offshore Hydromechanics*, First Edition. Mekelweg, Dutch, 2001.